

See discussions, stats, and author profiles for this publication at: <https://www.researchgate.net/publication/278393169>

Polymorphism of Anti-HIV Drug Efavirenz: Investigations on Thermodynamic and Dissolution Properties

ARTICLE in CRYSTAL GROWTH & DESIGN · OCTOBER 2014

Impact Factor: 4.89 · DOI: 10.1021/cg500509c

CITATIONS

3

READS

26

10 AUTHORS, INCLUDING:



[Cinira Fandaruff](#)

Federal University of Santa Catarina

8 PUBLICATIONS 13 CITATIONS

[SEE PROFILE](#)



[Carlos Eduardo Maduro de Campos](#)

Federal University of Santa Catarina

117 PUBLICATIONS 951 CITATIONS

[SEE PROFILE](#)



[Helvecio Rocha](#)

Fundação Oswaldo Cruz

15 PUBLICATIONS 47 CITATIONS

[SEE PROFILE](#)



[Gustavo Monti](#)

National University of Cordoba, Argentina

56 PUBLICATIONS 362 CITATIONS

[SEE PROFILE](#)

Polymorphism of Anti-HIV Drug Efavirenz: Investigations on Thermodynamic and Dissolution Properties

Cinira Fandaruff,[†] Gabriela S. Rauber,[†] Andrea M. Araya-Sibaja,[‡] Rafael N. Pereira,[†] Carlos E. M. de Campos,[§] Helvécio V. A. Rocha,^{||} Gustavo A. Monti,[†] Thaciana Malaspina,[#] Marcos A. S. Silva,[†] and Silvia L. Cuffini*,^{†,‡,#}

[†]Laboratório de Controle de Qualidade, Universidade Federal de Santa Catarina, Florianópolis, Santa Catarina 88040-900, Brasil

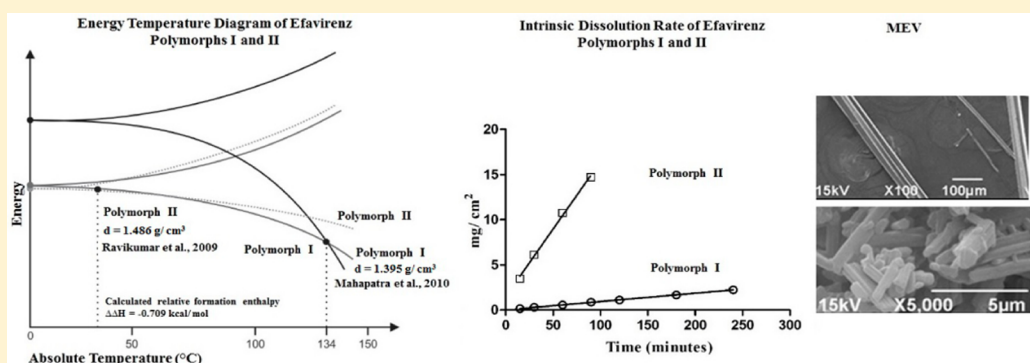
[‡]Escuela de Química, Universidad de Costa Rica, 2060, San José, Costa Rica

[§]Laboratório de Difração de Raio-X, Departamento de Física, Universidade Federal de Santa Catarina, Florianópolis, Santa Catarina 88040-900, Brasil

^{||}Laboratório de Sistemas Farmacêuticos Avançados, Instituto de Tecnologia em Fármacos/Farmanguinhos (FIOCRUZ), Rio de Janeiro, Rio de Janeiro 22775-610, Brasil

[#]FaMAF, Universidad Nacional de Córdoba & IFEG-CONICET, Córdoba 5000, Argentina

*Pós-Graduação em Engenharia e Ciências dos Materiais, Universidade Federal de São Paulo, São José dos Campos, São Paulo, 12231-280, Brasil



ABSTRACT: Polymorphs, cocrystals, solvates, and hydrates have been reported for efavirenz (EFV), which is part of high activity antiretroviral therapy (HAART), and it is considered to be the best choice in the treatment of adults and children. However, studies about thermodynamic stability and improvement of dissolution properties have been rarely reported for the anhydrous polymorphic forms. Therefore, the aim of this work was to characterize the solid state of anhydrous polymorph I and polymorph II (herein obtained), to study the thermodynamic stability and strategies to improve the dissolution properties. In addition, techniques such as, X-ray powder diffraction (XRPD), differential scanning calorimetry (DSC), hot stage microscopy (HSM), scanning electron microscopy (SEM), Fourier transform infrared (FT-IR), raman spectroscopy (RS), theoretical calculations, and solid-state nuclear magnetic resonance (ss-NMR) were used to complete this work. Thermodynamic studies showed that polymorphs I and II are enantiotropically related with the isoenergetic point between 35 and 40 °C. The Efv polymorph II showed itself to be more stable and 10-fold more soluble than polymorph I, due to modifications of morphology. Therefore, polymorph II could be an excellent candidate with significant advantages for pharmaceutical formulations.

1. INTRODUCTION

Efavirenz (EFV), (4S)-6-chloro-4-(2-cyclopropylethynyl)-4-(trifluoromethyl)-2,4-dihydro-1*H*-3,1-benzoxazin-2-one, belongs to the class of non-nucleoside reverse transcriptase inhibitors (NNRTI). It is manufactured by Bristol-Myers Squibb and Merck Sharp & Dohme as Sustiva and Stocrin, respectively, and was approved for the treatment of human immunodeficiency virus type 1 infection (HIV-1) in 1998.¹ It is part of high activity antiretroviral therapy (HAART), and it is considered to be the best choice in the treatment of adults and children.²

EFV belongs to class II of Biopharmaceutical Classification System (BCS); that is, it is poorly water-soluble and highly permeable.³ Due to its low solubility in water, significant differences in bioavailability can be observed in the various polymorphic forms of EFV.⁴ Recent studies have been related to cocrystals, solvates, and anhydrous polymorphic compounds of EFV (Table 1).^{5–8} However, studies about its thermody-

Received: April 13, 2014

Revised: August 4, 2014

Published: September 22, 2014

namic stability, improvement of dissolution properties and morphology effects in the IDR have been rarely reported.

Table 1. Polymorphs, Co-crystals, and Solvates of EFV

Polymorphs			
polymorph I ⁵	polymorph II ⁶	polymorph Ia ⁵	polymorph III ⁷
orthorhombic <i>P</i> 2 ₁ 2 ₁ 250 K	orthorhombic <i>P</i> 2 ₁ 2 ₁ 294 K	monoclinic <i>P</i> 2 ₁ 198 K	monoclinic C2 300 K
Cocrystals			
cocrystal with 1 ⁷		cocrystal with 2 ⁷	
form II ⁵	form IIa ⁵	form III ⁵	form IV ⁵
monoclinic C2 298 K	monoclinic C2 150 K lower temperature	monoclinic C2 150 K lower temperature	triclinic P1 298 K
Solvates			
hydrate ⁵		hydrochloride ⁸	
orthorhombic <i>P</i> 2 ₁ 2 ₁ 294 K		orthorhombic <i>P</i> 2 ₁ 2 ₁ 120 K	

The aim of this work was to characterize the solid state of anhydrous polymorphs I and II (herein obtained), to study the most stable phase at room temperature, and to find strategies to improve the dissolution properties. For that, X-ray powder diffraction (XRPD), differential scanning calorimetry (DSC), hot stage microscopy (HSM), scanning electron microscopy (SEM), Fourier transform infrared (FT-IR), Raman spectroscopy (RS), theoretical calculations, and solid-state nuclear magnetic resonance (ss-NMR) techniques were used to achieve a complete solid state characterization of both polymorphs.

2. EXPERIMENTAL SECTION

2.1. Samples. For confidential reasons, the manufacturer of the EFV raw material will not be reported herein. The EFV raw material is micronized, and it contains polymorph I, while the polymorph II is a recrystallized form.

2.2. Crystal Growth. Approximately 100 mg of EFV was dissolved in methanol in a stirring condition. After 15 min, the volume was completed to 50 mL in volumetric flasks. The solution was transferred to a beaker and allowed to evaporate slowly at freezing temperature for approximately 7 days to produce needles. The crystallization method employed in the present work is different from the method previously proposed by Ravikumar and Sridhar.⁶ However, we obtained the same crystal structure, which we call polymorph II.

2.3. Techniques for Characterization. **2.3.1. Scanning Electron Microscopy (SEM).** The morphology of the needles obtained was evaluated using SEM. The sample was mounted on metal stubs using double-sided adhesive tape, vacuum-coated with gold (350 Å) in a Polaron E-5000, and analyzed using a scanning electron microscope (Philips, Model XL 30) at a voltage of 15 kV, using magnification of 50× and 100×.

2.3.2. X-ray Powder Diffraction (XRPD). XRPD patterns were recorded at room and nonambient temperatures on a XPERT PANalytical diffractometer, equipped with X'Celerator detector, using Ni filtered $\text{K}\alpha$ radiation of a Cu tube operating with 40 kV and 45 mA. The Soller divergent and antiscattering slits used were 0.04 rad and 0.25°, respectively. XRPD measurements were carried out using 2θ range from 5° to 45° (and from 4° to 26° for nonambient runs), scan step size of 0.008°, and scan step time of 20 s. The samples were heated using an AntonPaar HTK16 camera from 25 to 134 °C and cooled to 25 °C at 10 °C/min rates, except during XRPD patterns acquisition (isotherms). The calculated XRPD pattern was carried out with a line width different from the experimental one.

2.3.3. Raman Spectroscopy (RS). Raman spectra were collected in backscattering geometry using a PeakSeeker 785 (RAM – PRO – 785) Raman system with a diode laser of 785 nm and 300 mW at the source. The collected Raman radiation was dispersed with a grating and focused on a Peltier-cooled charge-coupled device (CCD) detector allowing us to obtain a spectral resolution of 6 cm^{-1} . The LASER was focused on the sample by a 20× objective lens of a microscope giving a spot of approximately 2 μm diameter. All spectra were recorded in the spectral window of 200–1800 cm^{-1} with same acquisition time (30 s). The powders were analyzed in glass blades at room temperature.

2.3.4. Fourier Transform Infrared (FT-IR). FT-IR spectra of the sample were recorded on an IR Prestige-21 Shimadzu, mixed with KBr (potassium bromide), and analyzed in the range of 4000–600 cm^{-1} .

2.3.5. Solid-State Nuclear Magnetic Resonance (ss-NMR). High resolution ¹³C solid state spectra for both forms, polymorph I and polymorph II, were recorded using the ramp CP/MAS sequence with proton decoupling during acquisition. The solid state NMR experiments were performed at room temperature in a Bruker Avance II spectrometer operating at 300.13 MHz for protons and equipped with a 4 mm MAS probe. The operating frequencies for protons and carbons were 300.13 and 75.47 MHz, respectively. Adamantane was used as an external reference for the ¹³C spectra and to set the Harmann–Hahn matching condition in the cross-polarization experiments. Spinning rate was 10 kHz. The number of transients for each compound was 1024 for polymorph II and 2048 for polymorph I in order to obtain an adequate signal-to-noise ratio. The recycling time, the contact time during CP, and the acquisition time were 6 s, 2.0 ms, and 41 ms, respectively, for all the samples. SPINAL 64 sequence was used for decoupling during acquisition with a proton decoupling field H_{H} satisfying $\omega_{\text{H}}/(2\pi) = \gamma H_{\text{H}}/(2\pi) = 78.2$ kHz. Quaternary carbon edition spectra were recorded for all the samples. These spectra were acquired with the nonquaternary suppression (NQS) sequence, where the ¹H and ¹³C radio frequency (rf) fields are removed during 40 μs after CP and before the acquisition. This delay allows the carbon magnetization to decay because of the ¹H–¹³C dipolar coupling, resulting in spectra where CH and CH₂ are substantially removed. This experiment allows us, then, to identify quaternary carbon signals.

2.3.6. Differential Scanning Calorimetry (DSC). DSC curves of crystals produced were obtained in a DSC-60 cell (Shimadzu) using aluminum crucibles with about 1 mg of sample under a dynamic nitrogen atmosphere (50 mL/min) and heating rate of 10 °C/min in the temperature range from 30 to 250 °C. The DSC cell was calibrated with a standard reference of indium.

2.3.7. Hot-Stage Microscopy (HSM). Thermal events were observed on an Olympus BX50 microscope equipped with a Mettler Toledo FP-82 hot stage. The sample was placed on a microscope slide, covered with a coverslip, and heated at a rate of 5 °C min⁻¹.

2.3.8. Theoretical Calculations. Quantum chemistry calculations at density functional theory (DFT) level were performed to obtain the geometries of EFV polymorphs. The specific DFT used was the wB97X-D.⁹ The wB97X-D functional shows slight improvement over other empirical dispersion-corrected density functionals, while for covalent systems and kinetics, it performs noticeably better. Relative to our previous functionals, such as wB97X, the new functional is significantly superior for nonbonded interactions and very similar in performance for bonded interactions. Since wB97X-D is a parametrized functional, it was tested by the developers against three well-established existing DFT-D functionals (B97-D, B3LYP-D, and BLYP-D), as well as the previous LC hybrid functionals (wB97X and wB97) on a separate independent test set of data, which includes further atomization energies, reaction energies, noncovalent interaction energies, equilibrium geometries, and a charge-transfer excited state. The results of all these tests indicate that this new long-range corrected DFT-D functional is generally somewhat superior in overall performance. The basis function set used was 6-311++G(d,p),¹⁰ where addition of diffuse functions (symbolized by the++) as a polarization functions (d,p) improves the description of molecular systems. Geometry optimization was performed for the two polymorphic forms of EFV species using the quantum chemical level specified

before. The calculations were carried out with the Gaussian 03 suite of programs.¹¹ All degrees of freedom were optimized, and only positive vibrational frequencies were obtained at these optimized geometries at the wB97X-D/6-311++G(d,p) level. The relative order of stability of isomeric structures was obtained by the same theoretical level. The zero point energies (ZPE) were calculated from vibrational frequencies obtained from structures optimized at the wB97X-D level with the same basis set (6-311++G(d,p)). A detailed comparison of theoretical methods was not carried out at this point because it was outside the scope of our work. The IR spectra was obtained at wB97XD/6-311++G(d,p) theoretical level.

2.3.9. Intrinsic Dissolution Test. The method to quantify EFV in the determination of IDR was optimized and validated. In the method to quantify EFV to determine the IDR, the APIs (100 mg) were compacted in disks by using a hydraulic press with manometer ASTA to 400 kg and were analyzed in a VARIAN VK 7000 dissolution test system. This dissolution study refers to a USP method, which uses a compressed disk. The method is specified in USP30-NF25 1087 Intrinsic Dissolution.¹² The effect of pressure was controlled by DSC and XRPD, confirming there were no polymorphic transitions.

The dissolution medium selected was 200 mL of sodium lauryl sulfate (SLS) 0.25% (w/v) previously heated at 37 °C ± 0.5 °C. The USP specifications state dissolution media as 1% and 2% w/v of SLS for EFV. The addition of SLS 0.25% (w/v), in the maximum limit of CMC,¹³ was necessary to improve the wettability of EFV. The concentration of SLS chosen was 0.25%, because we considered this condition more biorelevant.^{14–18}

In order to ensure the sink condition, measurement of saturation concentrations was carried out until 96 h. The maintenance of sink conditions during the EFV IDR assays was ensured since the solubility after an equilibration period of 96 h was 239.75 ± 0.01 µg/mL for polymorph I and 316.63 ± 0.02 µg/mL for polymorph II. The concentration of the drug after 240 min in the IDR analysis was 4.49 µg/mL for polymorph I and 29.45 µg/mL after 90 min for polymorph II. The periods of IDR analysis were different in order to ensure the sink condition during all of the experiment for each polymorph. Therefore, the maximum concentration of the drug was lower than 10% of the solubility in the IDR dissolution medium.¹² The analyses were done in a rotation speed of 75 rpm, the apparatus 2 (USP)¹² was used, and the samples were withdrawn at 15, 30, 60, 90, 120, 180, and 240 min for polymorph I and until 90 min for polymorph II, which were replaced with an equal volume of the fresh medium to maintain a constant total volume. The sample aliquots were filtered and analyzed by high performance of liquid chromatography (HPLC). The chromatographic analyses were performed in a HPLC Shimadzu LC10AT equipped with a vacuum degasser DGU-10AL, detector UV-vis Shimadzu SPD-10Av, and self-injector Rheodyne 7125. The chromatograms were recorded in CLASS-VP software (version RV 6.14). A PerkinElmer C18 (150 mm × 4.6 mm, 5 µm) column was used. The mobile phase consisted in acetonitrile/ammonium acetate buffer pH 7.5 (50:50 v/v), flow rate of 1 mL/min, injection volume of 20 µL, and detection performed at 272 nm. The parameters of chromatographic system were used according to the United State Pharmacopeia (USP)¹² to EFV after covalidation. After the dissolution tests, the polymorphs I and II were controlled by XRPD and did not present transitions or modifications.

3. RESULTS AND DISCUSSION

3.1. Characterization of Polymorphs I and II.

3.1.1. Scanning Electron Microscopy (SEM). The images (Figure 1) could be visualized by increasing the magnification to 100× for polymorph II and 5000× for polymorph I. Polymorph I is micronized, while polymorph II is a recrystallized form; thus, different amplifications were used. Regular forms were observed for the EFV polymorph I, and the crystals were in columnar shape.¹² The images of polymorph II showed crystals in needle shape.

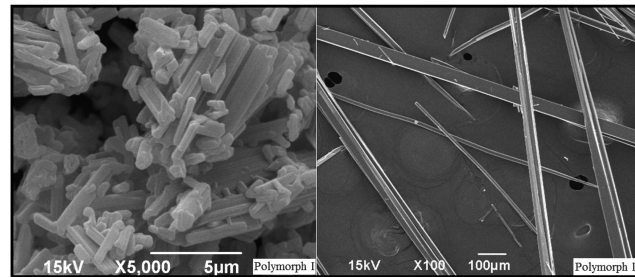


Figure 1. SEM of EFV polymorphs I and II.

3.1.2. X-ray Powder Diffraction (XRPD). The comparison between experimental XRPD of polymorph I and the calculated structure by Mahapatra et al.⁵ showed the same crystalline structure (Figure 2). On the other hand, the crystalline

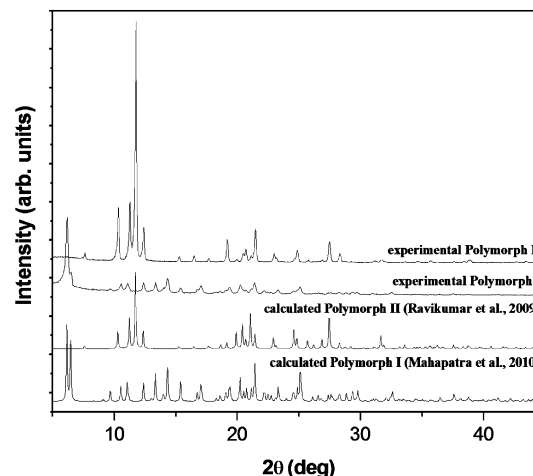


Figure 2. Comparison between experimental and calculated XRPD of EFV polymorphs I and II.

structure of polymorph II was identified with the previously described form by Ravikumar et al.⁶ The differences observed in the intensities between calculated and experimental data can be associated with the preferential orientation. Polymorph I crystallizes in the space group $P2_12_12$ with three molecules in the asymmetric unit.⁷ In the structure resolved by Ravikumar et al.⁸ and named by us polymorph II, the molecules crystallize in space group $P2_12_12_1$. A third polymorph reported by Melo et al.⁷ (Table 1) and named herein polymorph III crystallizes in the space group $C2$. Polymorph III shows the highest density value, $d = 1.501 \text{ g/cm}^3$, followed by polymorph II, $d = 1.486 \text{ g/cm}^3$, and polymorph I, $d = 1.395 \text{ g/cm}^3$.⁵ Polymorph I contains conformation type synthon A,⁵ while in polymorphs II and III the conformation type synthon C (see Figure 3) is present.⁷ The conformation type of synthon C justifies the higher density value of polymorphs II and III, as well as the presence of conformation type synthon A explains the noticeable degree of conformational disorder in the polymorph I.⁵

3.1.3. Raman Spectroscopy (RS) and Fourier Transform Infrared (FT-IR). Through RS and FT-IR, it was possible to compare the most important bands with the literature¹⁹ and to characterize the polymorphs of EFV. Figure 4a shows the Raman and FT-IR spectra obtained for the EFV polymorphs I and II. In this figure, clear differences between the two polymorphs are shown; notice how different their absorption

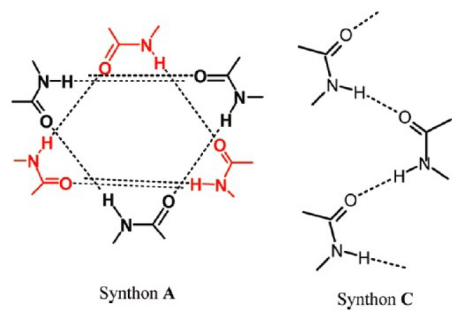


Figure 3. Synthon A and synthon C were reported by Mahapatra et al.⁵ EFV polymorph I presents synthon A, and EFV polymorphs II and III present synthon C.

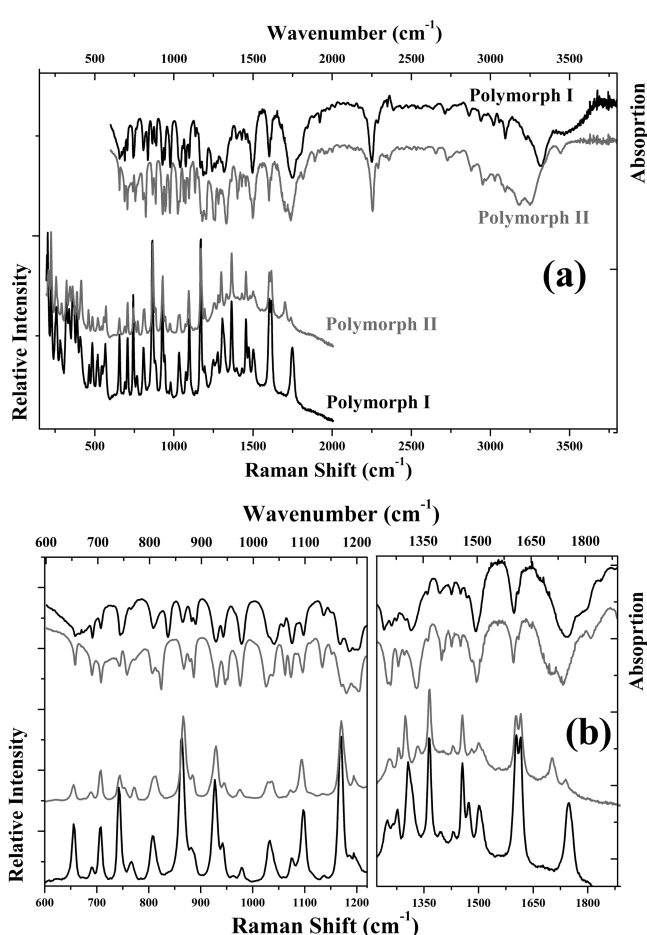


Figure 4. (a) Raman and IR absorption spectra of both polymorphic forms of EFV. (b) Detailed view of some spectral regions. The black and gray lines represent the polymorphs I and II, respectively.

spectra between 2800 and 3200 cm⁻¹ are. Around 1740 cm⁻¹, both Raman and IR absorption spectra showed two new lines for polymorph II. In Figure 4b, many other new Raman and IR optical active modes can be uncovered. In this figure, it is possible to confirm the difference between the spectra in the 1650 and 1850 cm⁻¹ region, to observe more differences in the 1235 and 1350 cm⁻¹ region, and also to see that many IR active modes are also Raman active modes. Furthermore, it can be noticed that the peak intensity in the RS spectrum of polymorph II is clearly smaller for the full spectral range examined. The main Raman lines and absorption bands shown in the RS and IR spectra of polymorph I are in agreement with

the literature;¹⁹ however, several differences in both RS and IR spectra were observed for polymorph II. This evidence inspired further studies that will be published soon.

3.1.4. Solid-State Nuclear Magnetic Resonance (ss-NMR).

Figure 5 shows the CP/MAS and NQS/MAS ¹³C spectra of both polymorphic forms. A tentative signal assignment is displayed in Table 2. Carbon numbering is according to Ravikumar et al.⁶ The ¹³C signal assignment was performed using the information obtained from the NQS experiment, taking into account the residual dipolar interaction between ¹³C and quadrupolar nuclei (¹⁴N, ^{35,36}Cl) and solution NMR experiments. The ¹³C spectrum of polymorph I shows more than one resonance form of carbon in the molecule, indicating that there is more than one molecule in the asymmetric unit. The three signals corresponding to C11 are clear indications of the presence of three molecules in the asymmetric unit. This fact is in agreement with X-ray data from Mahapatra et al.⁵

In the ¹³C CP/MAS spectrum of polymorph II, there is one resonance for each distinct ¹³C nucleus in the molecule. In accordance with Ravikumar et al.,⁶ there is only one molecule in the asymmetric unit. The C9 resonance is observed as a broad line centered around 128 ppm in polymorphs I and II. This broadening of the resonance is due to the dipolar coupling of C9 to the fluorine nuclei (the ¹³C spectra are only proton decoupled). Resonance lines at 135 and 149 (147 in polymorph I) ppm show the characteristic shape due to residual dipolar coupling interaction to ¹⁴N and ^{35,36}Cl quadrupolar nuclei, respectively.

It is noteworthy, in the NQS experiment for the polymorph I, that the resonances of the carbons belonging to the cyclopropyl group are not suppressed. A similar behavior usually occurs with methyl groups because the rotation of the group averages out the proton–carbon dipolar coupling, making the NQS experiment inefficient for those molecular groups. This fact suggests a high mobility of the cyclopropyl group. This is in agreement with the noticeable degree of conformational disorder reported for this group in polymorph I by Mahapatra et al.⁵ Actually we can say that the disorder, taking into account the NMR results, is of dynamical origin.

3.1.5. Thermal Analysis, Hot Stage Microscopy (HSM), and Nonambient Temperature X-ray Powder Diffraction (XRPD).

DSC data of EFV polymorph I are in agreement with the literature (Figure 6), which cites a melting point of about 138–140 °C.⁵ Raw materials samples have also been evaluated and the melting point was determined as 138.6 °C.²⁰ Another result of 137 °C was previously reported by da Costa et al.²¹ The DSC curve of polymorph II (needles) indicates a slight change in the melting point to 137.20 °C and moreover the appearance of another endothermic peak in 105.52 °C. This latest evidence suggests that both polymorphs present a solid–solid transition, since it was demonstrated by TG curve that the sample does not contain any residual solvent and no loss of mass was observed. The polymorphic solid-state transition was also confirmed by HT-XRPD and HSM. The fusion event was not observed up to 137 °C using HSM. In Figure 7, the observation by polarized light confirmed the solid–solid transition above 100 °C. Another verification of the polymorphic transition was done by HT-XRPD (Figure 8). The pattern corresponding to polymorph II was determined from 25 to around 100 °C. Above this temperature, the crystalline structure corresponds to polymorph I, in total agreement with DSC curves and HSM images. The small difference between the values of temperature transition (105 °C in HSM and 100 °C in the diffractometer)

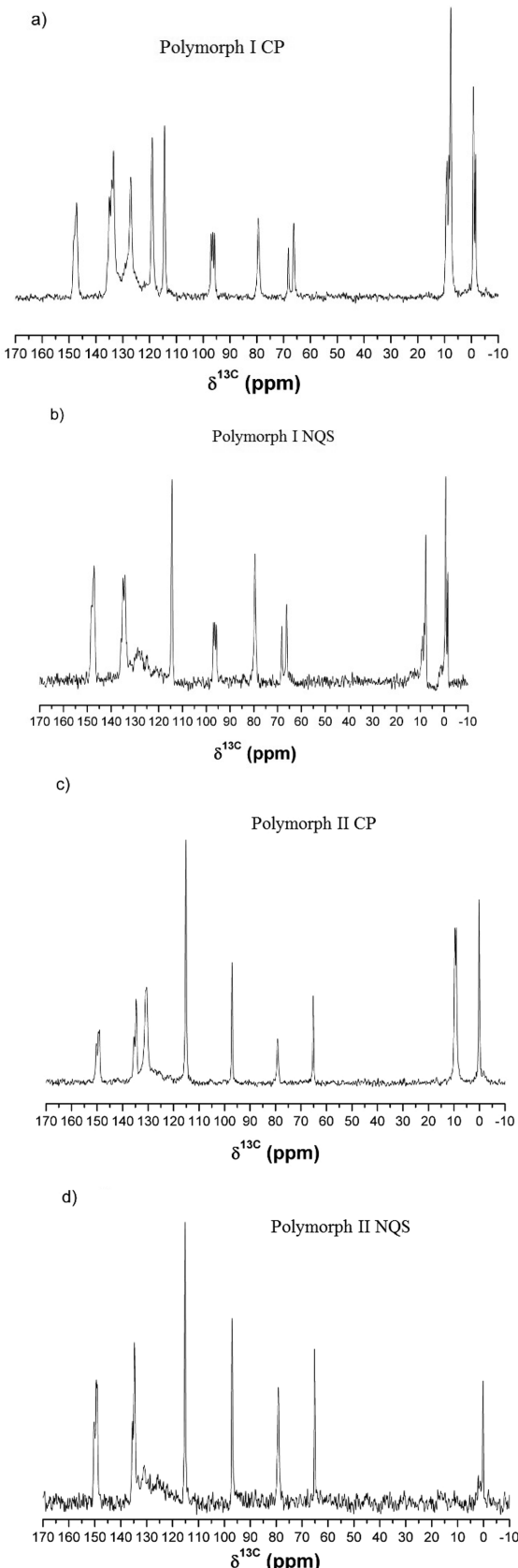


Figure 5. ^{13}C CP/MAS and NQS spectra of solid EFV polymorph I (a, b) and polymorph II (c, d).

can be justified because the first system is closed while the other one is opened. It is noteworthy that these studies were carried

Table 2. A Signal Assignment to Polymorph I and Polymorph II of EFV

carbon number	polymorph I chemical shift, δ (ppm)	polymorph II chemical shift, δ (ppm)
12	-1.5, -0.7	0.1
13, 14	7.7, 8.3, 9.1, 9.4	9.1, 9.7
10	66.2, 68.2	65.2
8	79.4	79.2
11	95.8, 96.4, 97.0	97.1
7	114.4	115.2
9	128.0	127.8
3, 4, 6	119.0, 127.0, 133.4	130.5, 131.0
5	135.0	135.0
2	147.3	149.2
1	148.0, 148.4	150.3

out in dry conditions, and therefore, the solid state transition occurs around 105 °C, which will be changed when solvent-mediated.^{22,23}

3.1.6. Stability Relationship between the EFV Polymorphs. According to Brittain²⁴ and Bernstein,²⁵ an enantiotropic system is characterized as a system in which a solid state transition can be observed at the temperature where both free energy curves cross. At that point, both forms are isoenergetic. Through the HSM, DSC, and HT-XRPD experiments in dry conditions, the transition from the polymorph II to the polymorph I around 105 °C was confirmed. The fact that the polymorph I density ($d = 1.395 \text{ g/cm}^3$) is less than the polymorph II density ($d = 1.486 \text{ g/cm}^3$) is in agreement with the fact that the polymorph II is more stable than polymorph I at room temperature.

Taking into account that these results were measured in dry conditions, the polymorphic transformation can occur directly in the solid state, but its rate is usually much lower than that of solvent-mediated transformation. This transformation was determined by suspending equal weights of both polymorphs at various temperatures in order to determine a narrow temperature range.^{22,23} After 3 days, the XRPD of the solid phase revealed that the true thermodynamic transition temperature was found between 35 and 40 °C. Based on this analysis, a schematic free energy versus temperature diagram was made and is shown in Figure 9. Therefore, polymorphs I and II are enantiotropically related with the isoenergetic point between 35 and 40 °C.

3.1.7. Theoretical Analyses. Theoretical calculations were carried out, and the minimum energy structures of the two studied EFV conformers of the different polymorphs were obtained theoretically at the wB97XD/6-311++G(d, p) level. The optimized molecular structures are shown in Figure 10.

The main molecular structural difference between the two optimized species was the dihedral angle formed by (H)CC(C) and ClC bonds. In EFV, conformer I of polymorph I showed a dihedral angle around 103.4°, whereas in conformer II of polymorph II, this same angle was around 167.2°. All the other structural parameters (bonds and angles) were very similar in both optimized EFV species. Vibrational analysis was performed to ensure that the calculated structures are real minima of the potential energy surfaces and also to obtain the zero point energy. The final energies were then evaluated for the final optimized geometry. All degrees of freedom were optimized, and only positive vibrational frequencies were obtained at these optimized geometries at the wB97XD/6-

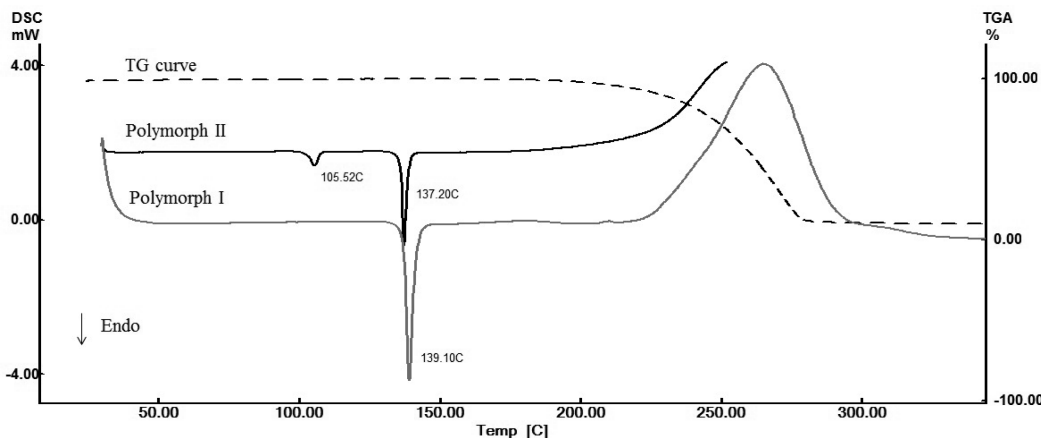


Figure 6. DSC curves of EFV polymorphs I and II and TG curve.

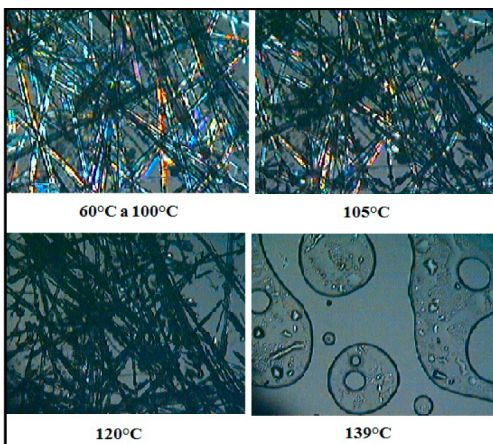


Figure 7. Melting behavior of EFV polymorph II. Polymorph II is stable until 100 °C, has a solid–solid transition at 105 °C, and melts at 139 °C.

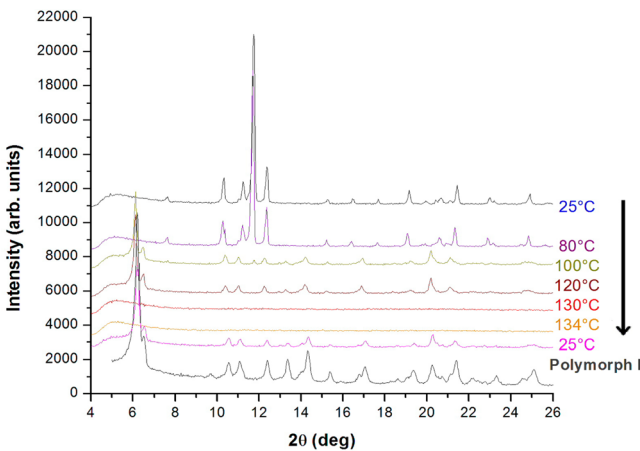


Figure 8. Heating of polymorph II from 25 to 134 °C and cooling to 25 °C. The arrow indicates the direction which the measurements were carried out.

311++G(d,p) level. The EFV conformer II (polymorph II) was more stable than conformer I (polymorph I). The energy difference between the two species is very small, on the order of kT (~ 0.6 kcal/mol), about 0.23 kcal/mol. Similarly, Ayala and co-workers¹⁹ obtained an energy difference for these two conformers, calculated at the B3LYP/6-311++G(d,p) level, as

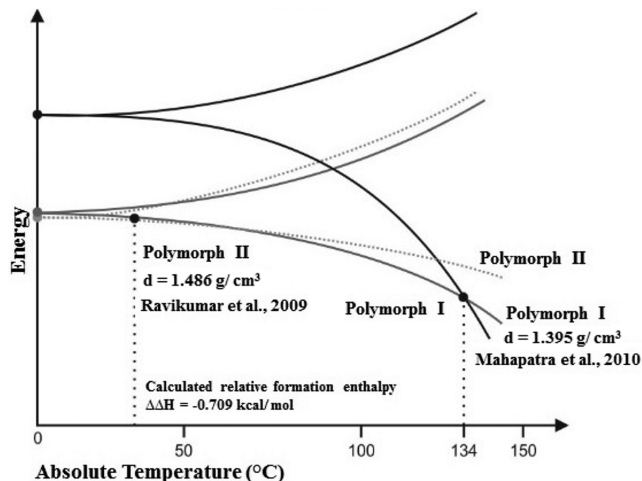


Figure 9. Schematic free energy versus temperature diagram of EFV polymorphs I and II. The calculated relative formation enthalpy points to polymorph II as the most stable.

0.226 kcal/mol (ΔH). Our calculations for the same energy difference indicate the relative enthalpy of formation as $\Delta\Delta H = -0.709$ kcal/mol in favor of conformer II (polymorph II) as the most stable conformer. Due to this small difference in the total energy systems, including corrections to the zero point vibrational energy (ZPE), it is believed that both species are equally probable to be obtained experimentally. The reference value for the energy of the species of EFV takes into account the zero-point correction to the total energy of this species, $E = -1503.530786$ hartree. If the value of this energy obtained for zero point correction, 0.207930 hartree, were deducted, the value of electronic energy, -1503.738716 hartree, would be obtained, in agreement with the value previously obtained by Mahapatra and coauthors⁵ ($E = -1503.8168$ hartree, obtained at B3LYP/6-31++G(d,p) level). The difference between our value and the value in the literature for the total energy is justified due, in the major part, to inclusion of the zero-point energy correction in our calculation of the total energy value. Moreover, it is expected that these values are slightly different because they were obtained with different theoretical levels, methods, and basis functions for the two energies values. The infrared spectra of the EFV polymorphs I and II were obtained at wB97XD/6-311++G(d,p) theoretical level. No significant differences between the spectra of EFV polymorphs I and II

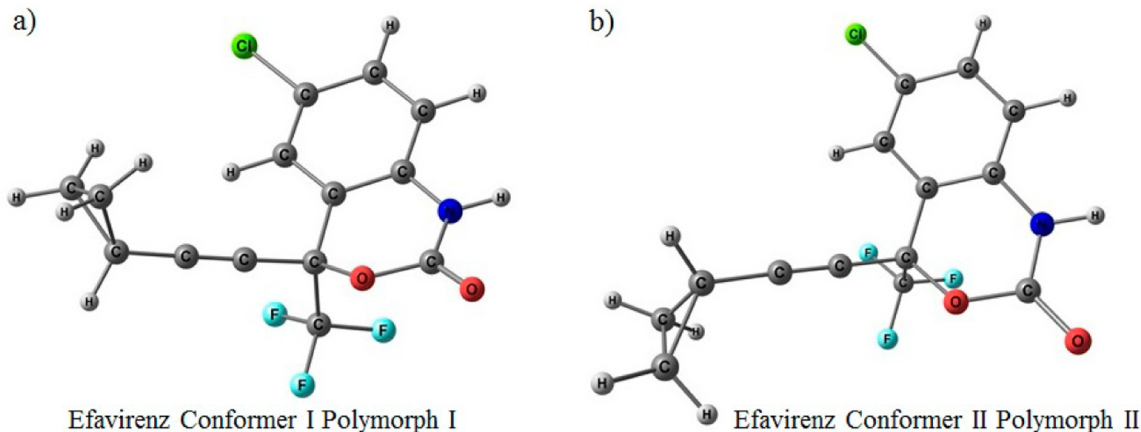


Figure 10. Structures obtained by the geometry optimization at wB97XD/6-311++G(d, p) level: (a) EFV conformer I, polymorph I; (b) EFV conformer II, polymorph II.

were noticed. This behavior had also been observed in the spectra obtained experimentally.

According to the previous experimental results, polymorph II is more stable than polymorph I at room temperature. However, the energy difference between the two conformers is very small, about 0.226 kcal/mol, including enthalpic correction. Therefore, the solid intermolecular interactions of conformation type synthon C in the polymorph II would stabilize the crystalline structure with the highest density (polymorph I density⁵ = 1.395 g/cm³ and polymorph II density⁶ = 1.486 g/cm³). It is well-known that the highest density corresponds to highest thermodynamic stability.^{24,25}

3.1.8. Intrinsic Dissolution Rate (IDR). EFV, as a class II drug with low solubility and high permeability, presents a good correlation between in vivo results and dissolution tests. Therefore, the dissolution rate is the primary limiting aspect to be controlled since it determines the drug absorption.^{26,27} The surfactant SLS is indicated by USP¹² and Marques²⁸ to be used for poorly soluble drugs. EFV is insoluble in water; therefore SLS 0.25% was used as medium for the dissolution test in order to improve the wettability.

Figure 11 shows the intrinsic dissolution profile from polymorph I and polymorph II in SLS 0.25%. Statistical

Table 3. Equation and r^2 Obtained by Least-Square Linear Regression of Dissolution Tests and IDR to EFV Polymorphs I and II

sample	equation	r^2	IDR (mg·cm ⁻² ·min ⁻¹)
polymorph I	$y = 0.009x + 0.02427$	0.99987	0.009
polymorph II	$y = 0.149x + 1.49276$	0.99691	0.149

that there is no polymorphic phase transition mediated, neither by solvent nor by pressure.

The intrinsic dissolution studies indicate that probably different crystal planes are exposed by polymorph II in comparison with polymorph I, modifying the dissolution rate of the different polymorphs.^{29,30} This effect also might have a relevant impact in the bioavailability of the drug.

4. CONCLUSION

EFV polymorphs I and II were completely characterized by solid state techniques, XRPD, DSC, HSM, SEM, FT-IR, RS, ss-NMR, and theoretical calculations. Thermodynamic studies showed that these polymorphs are enantiotropically related, and EFV polymorph II is more stable in comparison with polymorph I at room temperature since the isoenergetic point is between 35 and 40 °C. However, the intrinsic dissolution rate of polymorph II is higher than that of polymorph I by more than 10-fold. Therefore, EFV polymorph II is the most stable form (thermodynamic property), and the morphology modification allows the increasing of its dissolution rate (kinetic property). In this work, we reported a very promising solid state form for formulations of EFV since polymorph II is as stable as polymorph I but significantly more soluble. This knowledge has fundamental relevance to the pharmaceutical industry, since the polymorph II could be an excellent candidate with noticeable advantages in relation to the currently used drug.

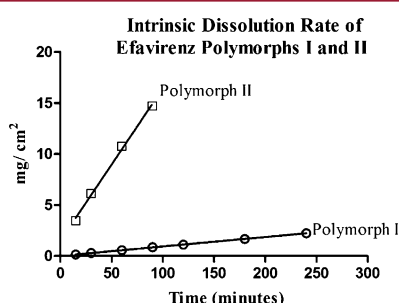


Figure 11. Intrinsic dissolution profiles of EFV polymorphs I and II.

analysis was carried out applying regression analysis and revealed that both polymorphs provided significantly different profiles (for confidence interval $\alpha = 0.05$, $p < 0.1$). Table 3 shows a very relevant result, since the IDR of polymorph II ($0.149 \text{ mg} \cdot \text{cm}^{-2} \cdot \text{min}^{-1}$) is over 10-fold higher than that of polymorph I ($0.009 \text{ mg} \cdot \text{cm}^{-2} \cdot \text{min}^{-1}$). The DSC and XRPD analyses, performed before and after the IDR essays, indicated

AUTHOR INFORMATION

Corresponding Author

*E-mail: scuffini@unifesp.br.

Notes

The authors declare no competing financial interest.

ACKNOWLEDGMENTS

The authors greatly appreciate the discussion of the results and the valuable suggestions from Professor Dr. Joel Bernstein. The XRPD and SEM measurements were performed at Laboratório de Difração de Raios-X (LDRX) and Laboratório Central de Microscopia Eletrônica (LCME) at UFSC. For the financial support for the development of the present study, the authors acknowledge CNPq, CAPES, FAPESC, CLAF, Fundación Sauberan, and PDTIS/FIOCRUZ.

REFERENCES

- (1) de Aquino, R. J. A.; de Campos, L. M. M.; Alves, R. J.; Lages, G. P.; Pianetti, G. A. Efavirenz related compounds preparation by hydrolysis procedure: Setting reference standards for chromatographic purity analysis. *J. Pharm. Biomed. Anal.* **2007**, *43*, 298–303.
- (2) Chiappetta, D. A.; Alvarez-Lorenzo, C.; Rey-Rico, A.; Taboada, P.; Concheiro, A.; Sosnik, A. N-Alkylation of poloxamines modulates micellar assembly and encapsulation and release of the antiretroviral efavirenz. *Eur. J. Pharm. Biopharm.* **2010**, *76*, 24–37.
- (3) Amidon, G. L.; Lennernäs, H.; Shah, V. P.; Crison, J. R. A theoretical basis for a biopharmaceutic drug classification: The correlation of in vitro drug product dissolution and in vivo bioavailability. *Pharm. Res.* **1995**, *12* (3), 413–420.
- (4) Perold, Z.; Swanepoel, E.; Brits, M. Anomalous dissolution behaviour of a novel amorphous form of Efavirenz. *Am. J. PharmTech Res.* **2012**, *2* (2), 2249–3387.
- (5) Mahapatra, S.; Thakur, S. T.; Joseph, S.; Varughese, S.; Desiraju, G. R. New Solid State Forms of the Anti-HIV Drug Efavirenz. Conformational Flexibility and High Z' Issues. *Cryst. Growth Des.* **2010**, *10*, 3191–3202.
- (6) Ravikumar, K.; Sridhar, B. Molecular and Crystal Structure of Efavirenz, a Potent and Specific Inhibitor of HIV-1 Reverse Transcriptase, and Its Monohydrate. *Mol. Cryst. Liq. Cryst.* **2009**, *515*, 190–198.
- (7) Melo, A. C. C.; Amorim, I. F.; Cirqueira, M. L. Toward Novel Solid-State Forms of the Anti-HIV Drug Efavirenz: From Low Screening Success to Cocrystals Engineering Strategies and Discovery of a New Polymorph. *Cryst. Growth Des.* **2013**, *13*, 1558–1569.
- (8) Cuffini, S.; Howie, R. A.; Tiekkink, E. R. T.; Wardell, J. L.; Wardell, S. M. S. V. (S)-6-Chloro-4-cyclopropylethynyl-4-trifluoromethyl-1H-3,1-benzoxazin-2(4H)-one. *Acta Crystallogr.* **2009**, *E65*, o3170–o3171.
- (9) Chai, J. D.; Head-Gordon, M. Long-range corrected hybrid density functionals with damped atom–atom dispersion corrections. *Phys. Chem. Chem. Phys.* **2008**, *10*, 6615–6620.
- (10) McLean, A. D.; Chandler, G. S. Contracted Gaussian basis sets for molecular calculations. I. Second row atoms, Z=11–18. *J. Chem. Phys.* **1980**, *72*, 5639–5648.
- (11) Frisch, M. J.; Trucks, G. W.; Schlegel, H. B.; Scuseria, G. E.; Robb, M. A.; Cheeseman, J. R.; Montgomery, J. A., Jr.; Vreven, T.; Kudin, K. N.; Burant, J. C.; Millam, J. M.; Iyengar, S. S.; Tomasi, J.; Barone, V.; Mennucci, B.; Cossi, M.; Scalmani, G.; Rega, N.; Petersson, G. A.; Nakatsuji, H.; Hada, M.; Ehara, M.; Toyota, K.; Fukuda, R.; Hasegawa, J.; Ishida, M.; Nakajima, T.; Honda, Y.; Kitao, O.; Nakai, H.; Klene, M.; Li, X.; Knox, J. E.; Hratchian, H. P.; Cross, J. B.; Bakken, V.; Adamo, C.; Jaramillo, J.; Gomperts, R.; Stratmann, R. E.; Yazayev, O.; Austin, A. J.; Cammi, R.; Pomelli, C.; Ochterski, J. W.; Ayala, P. Y.; Morokuma, K.; Voth, G. A.; Salvador, P.; Dannenberg, J. J.; Zakrzewski, V. G.; Dapprich, S.; Daniels, A. D.; Strain, M. C.; Farkas, O.; Malick, D. K.; Rabuck, A. D.; Raghavachari, K.; Foresman, J. B.; Ortiz, J. V.; Cui, Q.; Baboul, A. G.; Clifford, S.; Cioslowski, J.; Stefanov, B. B.; Liu, G.; Liashenko, A.; Piskorz, P.; Komaromi, I.; Martin, R. L.; Fox, D. J.; Keith, T.; Al-Laham, M. A.; Peng, C. Y.; Nanayakkara, A.; Challacombe, M.; Gill, P. M. W.; Johnson, B.; Chen, W.; Wong, M. W.; Gonzalez, C.; Pople, J. A. *Gaussian 03*, revision D.01; Gaussian, Inc.: Wallingford, CT, 2003.
- (12) *Optical Microscopy*, 30th ed.; USP, The United States Pharmacopeia: Rockville, MD, USA, 2007.
- (13) Ruddy, S. B.; Matuszewska, B. K.; Grim, Y. A.; Ostovic, D.; Storey, D. E. Design and characterization of a surfactant-enriched tablet formulation for oral delivery of a poorly water-soluble immunosuppressive agent. *Int. J. Pharm.* **1999**, *182*, 173–186.
- (14) Panikuar, A. D.; Venkat, R. Y.; Sunitha, G.; Sathesh, B. P. R.; Subrahmanyam, C. V. S. Development of Biorelevant and Discriminating Method for Dissolution of Efavirenz and its formulations. *Asian J. Pharm. Clin. Res.* **2012**, *5* (3), 220–223.
- (15) Guo, J.; Elzinga, P. A.; Hageman, M. J.; Herron, J. N. Rapid Throughput Solubility Screening Method for BCS Class II Drugs in Animal GI Fluids and Simulated Human GI Fluids Using a 96-Well Format. *J. Pharm. Sci.* **2009**, *97* (4), 1427–1442.
- (16) MacGregor, K. J.; Embleton, J. K.; Lacy, J. E.; Perry, E. A.; Solomon, L. J.; Seager, H.; Pouton, C. W. Influence of lipolysis on drug absorption from the gastro intestinal tract. *Adv. Drug Delivery Rev.* **1999**, *25*, 33–46.
- (17) Singla, N.; Gupta, G. D.; Kohli, K.; Singla, A. K. A Discriminatory and Biorelevant Dissolution Test Method for Simvastatin Drug Products. *Dissolution Technol.* **2009**, No. November, 11–13.
- (18) Zoeller, T.; Klein, S. Simplified Biorelevant Media for Screening Dissolution Performance of Poorly Soluble Drugs. *Dissolution Technol.* **2007**, No. November, 8–13.
- (19) Mishra, S.; Tandon, P.; Ayala, A. P. Study on the structure and vibrational spectra of efavirenz conformers using DFT: Comparison to experimental data. *Spectrochim. Acta, Part A* **2012**, *88*, 116–123.
- (20) Fandaruff, C.; Araya-Sibaja, A. M.; Pereira, R. N.; Hoffmeister, C. R. D.; Rocha, H. V. A.; Silva, M. A. S. Thermal behavior and decomposition kinetics of efavirenz under isothermal and non-isothermal conditions. *J. Therm. Anal. Calorim.* **2014**, *115*, 2351–2356.
- (21) da Costa, M.; Seiceira, R.; Rodrigues, C.; Hoffmeister, C.; Cabral, L.; Rocha, H. V. A. Efavirenz Dissolution Enhancement I: Co-Micronization. *Pharmaceutics* **2013**, *5*, 1–22.
- (22) Gu, C.; Grant, D. J. W. Estimating the Relative Stability of Polymorphs and Hydrates from Heats of Solution and Solubility Data. *J. Pharm. Sci.* **2001**, *90* (9), 1277–1287.
- (23) Zhang, G. G. Z.; Gu, C.; Zell, M. T.; Burkhardt, R. T.; Munson, E. J.; Grant, D. J. W. Crystallization and Transitions of Sulfamerazine Polymorphs. *J. Pharm. Sci.* **2002**, *91* (4), 1089–1100.
- (24) Brittain, H. G. Theory and Principles of Polymorphic Systems. In *Polymorphism in Pharmaceutical Solids*; Brittain, H. G., Ed.; Informa Healthcare USA: New York, 2009; pp 1–23.
- (25) Bernstein, J. Fundamentals. *Polymorphism in Molecular Crystals*; Oxford University Press: United Kingdom, 2002; pp 29–65.
- (26) Dressman, J. B.; Reppas, C. In vitro–in vivo correlations for lipophilic, poorly water-soluble drugs. *Eur. J. Pharm. Sci.* **2000**, *11* (2), S73–S80.
- (27) Rossi, R. C.; Dias, C. L.; Bajerski, L.; Bergold, A. M.; Fröhlich, P. E. Development and validation of discriminating method of dissolution for fosamprenavir tablets based on in vivo data. *J. Pharm. Biomed. Anal.* **2011**, *54*, 439–444.
- (28) Marques, M. R. C. Dissolução de Medicamentos. In *Ciências Farmacêuticas: Biofarmacotécnicas*; Storpirtis, S., Gonçalves, J. E., Chiann, C., Gai, M. N., Eds.; Guanabara Koogan S. A.: Rio de Janeiro, 2009; pp 96–108.
- (29) Kuminek, G.; Rauber, G. S.; Riekes, M. K.; Campos, C. E. M.; Monti, G. A.; Borloluzzi, A. J.; Cuffini, S. L.; Cardoso, S. G. Single crystal structure, solid state characterization and dissolution rate of terbinafine hydrochloride. *J. Pharm. Biomed. Anal.* **2013**, *78–79*, 105–111.
- (30) Danesh, A.; Connell, S. D.; Davies, M. C.; Roberts, C. J.; Tendler, S. J. B.; Willians, P. M.; Wilkins, M. J. An *In Situ* Dissolution Study of Aspirin Crystal Planes (100) and (001) by Atomic Force Microscopy. *Pharm. Res.* **2001**, *18* (3), 299–303.